VII International Conference on Computational Methods in Marine Engineering
MARINE 2017
M. Visonneau, P. Queutey and D. Le Touzé (Eds)

# SHIP RESISTANCE PREDICTION: VERIFICATION AND VALIDATION EXERCISE ON UNSTRUCTURED GRIDS

**P. CREPIER***

*Maritime Research Institute Netherlands (MARIN)
P.O. Box 28
6700 AA Wageningen, The Netherlands
e-mail: p.crepier@marin.nl, web page: http://www.marin.nl

**Key words:** CFD, KVLCC2, Verification, Validation, Double-body, Unstructured grid

**Abstract.** The prediction of the resistance of a ship is, together with the propeller performance prediction, part of the key aspects during the design process of a ship, as it partly ensures the quality of the power-prediction. Body fitted structured grids for ship simulations can be rather challenging and time consuming to build, especially when dealing with appended ship geometries. For this reason, unstructured hexahedral trimmed grids are more and more used. Such grids can be build by various CFD package such as CD-Adapcos Star CCM+, NUMECAs Hexpress grid generator or OpenFOAMSs SnappyHexMesh. Although their use is increasing or even already adopted, the numerical uncertainty of these simulations seems to be a well-kept secret.

In the study presented, an attempt at quantifying the numerical uncertainty of the resistance for the combination of the RANS Solver ReFRESCO [1] with grids generated using the commercial package Hexpress is made. The studied case is the flow around the bare-hull KVLCC2 at model scale Reynolds number. Extensive verification and validation on the same test case has already been published for the combination of ReFRESCO and structured grids by Pereira et al. [2].

The method to generate grids as geometrically similar as possible is presented, and the uncertainty analysis by L. Eça and M. Hoekstra [3] is performed on the integral results obtained. The simulations are performed using the $k-\omega$ $SST$, $k-\omega$ $TNT$ and the $k-\sqrt{k}L$ turbulence models. The velocity fields calculated in the propeller plane are compared to the measured ones and to the results obtained by Pereira et al. [2] on structured grids.

The results show that the differences with the experimental results are in the same range as the differences obtained with structured grids. The numerical uncertainties are, however, higher. They are also strongly dependent on the turbulence model used, like for structured grids, and are spread between 1.3% and 12%.

Concerning the wake flow details, not all features present in the experimental results are obtained and, compared to structured grids, the flow features are smoothed. The wake flow is also influenced by the turbulence modelling and needs to be adressed in more detail.

## 1 INTRODUCTION

Ship resistance predictions by means of Computational Fluid Dynamic (CFD) simulations is progressively taking over ship model testing, especially in the early design stages of the design loop. This sort of calculations has nearly become daily routine, but the accuracy of the results is often overlooked. While a lot of effort is spend during workshops, like the Gothenburg or Tokyo workshops, to gather validation material for various types of calm-water flows, not so much publications about verification of the simulations performed is available. Verification and Validation are two entirely different exercises as explained by Roache [4]: Verification is a mathematical exercise that aims at showing that we are solving the equations right, and validation is an engineering exercise to show that we are solving the right equations.

For ship flow simulation it is common to use body-fitted hexahedral trimmed meshes because they are easy to set-up even for complex geometries like appended ships. Such grids can be built by most of the popular CFD software package like CD-Adapco's Star CCM+, NUMECA's Hexpress or OpenFOAMS's SnappyHexMesh.

L. Eça and M. Hoekstra [3] proposed a method to estimate the numerical uncertainty of numerical simulations based on grid refinement studies of geometrically similar grids. Generating the appropriate sets of grids is straightforward when using structured grids but it becomes more challenging when working with unstructured meshes. This is most likely one of the main reasons for the lack of verification studies, in addition to being a rather costly exercise.

In the present study, the point of interest is the flow around the KVLCC2 at model scale for which plenty of data is available. The grid sets are built using NUMECAs grid generator Hexpress. In section 2 a summary of the test case and in-depth details about the method used to generate grids which are as geometrically similar as the grid generator allows. The details about the RANS solver and numerical settings are provided in section 3. In section 4, the obtained results are detailed in terms of numerical convergence, and the uncertainty analysis is performed on the resistance components. The details of the wake flow are also shown. These results are also compared to those obtained by Pereira et al.[2] for the same test case but with structured grids. Finally, in section 5, the conclusions of the findings are summarised.

## 2 GEOMETRY AND GRID GENERATION METHOD

### 2.1 KVLCC2

The object of the present study is the KVLCC2. A summary of its main particular, scale ratio and Reynolds number are provided in table 1 and a side view of the vessel is shown in figure 1.

**Figure 1**: Side view of the KVLCC2

**Table 1**: Main particulars of the KVLCC2

| Particular | Symbol | Value | Unit |
|---|---|---|---|
| Length between perpendiculars | $L_{pp}$ | 320.0 | [m] |
| Width | $B$ | 58.0 | [m] |
| Draught | $T$ | 10.8 | [m] |
| Scale | $\lambda$ | 58.0 | [-] |
| Froude Number | $F_r$ | 0.142 | [-] |
| Reynolds Number | $R_e$ | $5.80 \times 10^6$ | [-] |

### 2.2 Isotropic volume grid generation

The grids used in this study are so called trimmed meshes. In these meshes, a background grid with large cells is defined and then, the cells intersecting the input geometry are successively divided into 8 smaller cells to adapt to the details of the geometry. The main user input is the cell size for the initial grid, the refinement degree for each geometrical feature that should be captured, and the size of the transition zone between two refinement levels called diffusion depth d. Once a sufficient resolution is obtained at the places of interest, an anisotropic sub-layer of cells can be inserted to provide a grid suited to properly capture the boundary-layer on the walls present in the grid. The grid sets built for this study are based on an initial coarse grid which is successively refined to obtain, in total, five grids. To obtain grids that are as geometrically similar as possible the following method is used:

1. The initial cell size is decreased by a factor 2, 3, 4 and 5 in each direction by using 2,3,4 or 5 times more cells in each direction.

2. The surface refinement degree is kept constant throughout the sets: if, for instance, 6 refinements levels are set in the initial coarse grid, the same 6 successive refinements are performed for the other grids.

3. The size of the transition region, so-called diffusion depth d, is adapted such that it matches the expected final size of the grid. Details of the values used to generate the grids used in this study are provided in section 2.4

4. The anisotropic sub-layer settings are adapted to account for the refinement performed. This step is detailed in paragraph 2.3.

Examples of the volume obtained grid after the third step are shown in figure 2 for a simple case.

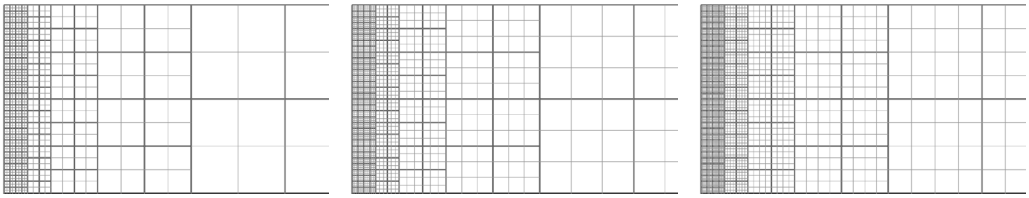

(a) 2 refinement levels (b) 3 refinement levels (c) 4 refinement levels

**Figure 2**: Example of volume grid refinement. Black lines : initial coarse grid ; Grey lines : refined grid

### 2.3 Anisotropic sub-layer grid generation

The size of the cells inserted in the anisotropic sub-layer follows a geometric series of first term S0 ,corresponding to the first cell size, and ratio r. The size of the $n^{th}$ cell is then defined as follow:

$$S_n = S_0 r^n \tag{1}$$

With such a definition, dividing the initial cell size, and keeping the ratio constant in all grids will not result in geometrically similar meshes. As shown in figure 3(a), when dividing the first cell size by two and keeping the ratio constant, between 13 and 14 cells are required to obtain a distance covered by 10 cells with the initial settings instead of 20.

To obtain geometrically similar grids, both the first cell size and and ratio should be adapted following Equations 2 and 3:

$$S_n = S_0 \frac{1 - r_1^{\frac{1}{n}}}{1 - r_1} \tag{2}$$

$$r_n = r_1^{\frac{1}{n}} \tag{3}$$

Where $S_0$ and $r_1$ are respectively the first cell size and growth ratio in the initial coarse grid, $S_n$ and $r_n$ the first cell size and growth ratio for the grid refinement $n$, $n = 1$ corresponding the coarsest grid.

Using the example in Figure 3(a) and setting up the geometric series properly, twice more cells are required with a refinement of 2 and 3 times more cells with a refinement 3, as shown in Figure 3(b).

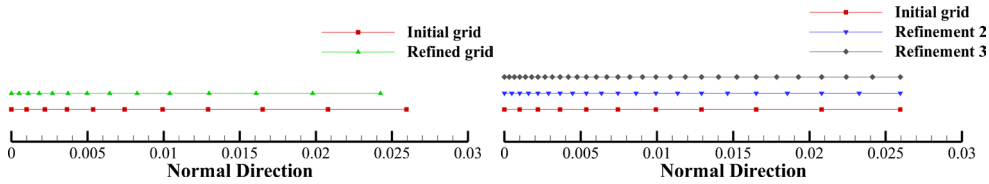


(a) Erroneous refinement (b) Geometrically similar refinement

**Figure 3**: Anisotropic sub-layer refinement set-up

### 2.4 Grid sets

Following the method described, two grid sets have been built. The sets differ only by the first cell size which is smaller in the second set, the isotropic volume grids are identical in both sets. All the grids built are 6 ship lengths long (3 astern, 2 ahead) and 2 ship lengths wide and deep. The ship geometry is split in 5 different parts, aft-ship, mid-ship, bilge, fore-ship and bulbous bow, to properly set-up the surface refinements. A box of volume refinement is used around the whole ship to keep the grid density reasonable near the ship.

Views of the CFD domain, surfaces and boxes defined around the ship are shown in figure 4. In table 2, details of the settings used for each surface patch and the box are provided.

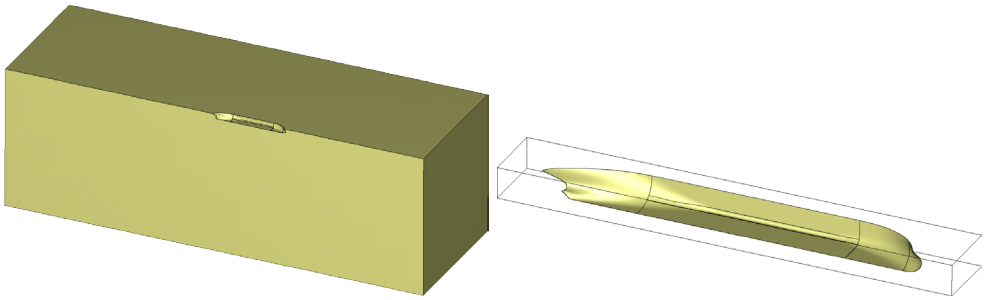

(a) Domain (b) Zones

**Figure 4**: CFD domain and definition of the surfaces and box around the ship

**Table 2**: Refinement levels set for each part of the grid

| Part | Aft-ship | Mid-ship | Bilge | Fore-ship | Bulbous Bow | Box ship |
|---|---|---|---|---|---|---|
| Level | 7 | 6 | 7 | 7 | 8 | 6 |

As detailed in section 2.2, to perform the refinement of the isotropic volume grid, only the number of cells in the initial grid and the transition layer are adapted. Details of the settings used to build the 5 grids per set are detailed in table 4. The growth ratio in the anisotropic sub-layer, which starts at 1.2 in the coarsest grids, is also adapted accordingly to the refinement level of each grids. The number of cells obtained in each grid, as well as the average $Y^+$ obtained with the $k-\omega\ SST$ turbulence model, are presented in table 3.

## 3 RANS SOLVER AND NUMERICAL SETTINGS

The simulations are performed using the URANS (Unsteady Reynolds Average Navier Stokes) CFD code ReFRESCO [1]. The QUICK scheme is used for the discretisation of the convective flux in the momentum equations. Three different turbulence models are used in this study, namely the $k-\omega\ SST$ [5],$k-\omega\ TNT$ [6] and the $k-\sqrt{k}L$ [7]. Upwind is used for the convective flux discretisation in the turbulence equations.

**Table 3**: Total number of cells in each grid in million and average $y^+$

| Grid set | 1 | | 2 | |
|---|---|---|---|---|
| | Cell count | $\overline{y_2^+}$ | Cell count | $\overline{y_2^+}$ |
| Grid 1 | 0.405 | 0.60 | 0.541 | 0.062 |
| Grid 2 | 2.79 | 0.30 | 3.826 | 0.030 |
| Grid 3 | 8.53 | 0.19 | 11.9 | 0.020 |
| Grid 4 | 19.1 | 0.14 | 27.1 | 0.015 |
| Grid 5 | 35.8 | 0.12 | 51.3 | 0.012 |

**Table 4**: Number of cells in the three directions and diffusion depth values used for the grid sets

| Grid | 1 | 2 | 3 | 4 | 5 |
|---|---|---|---|---|---|
| Nx | 12 | 24 | 36 | 48 | 60 |
| Ny | 4 | 8 | 12 | 16 | 20 |
| Nz | 4 | 8 | 12 | 16 | 20 |
| d | 1 | 3 | 5 | 7 | 9 |

As boundary condition of the problem, an inflow condition is imposed at the plane upstream of the ship and an outflow (Neumann) at the plane downstream. Symmetry conditions are imposed at the symmetry plane of the ship and at the top boundary. A constant pressure is imposed at the bottom and far-field left side of the ship. On the ship it self, a no-slip condition is used as the grid sets built are contracted enough towards the wall such that no wall functions are used.

## 4 RESULTS

### 4.1 NUMERICAL CONVERGENCE

In most of the simlations performed, all residuals are, on average, converged below $10^{-6}$ except for a few simulations where usually one of the turbulence quantities stagnates at a higher level of $10^{-4}$. This is especially true for the simulation with the $k-\omega$ based model where the $\omega$ becomes more difficult to solve when the grid is refined.

The results show that the residuals of the continuity and momentum equations are highest around the propeller plane while the turbulence residuals are highest at the bow of the ship. Figure 5(a) shows the convergence history of the root mean square residual for a case converging properly, and figure 5(b) for a stagnating case. Both figures are for the $k-\omega$ $SST$ turbulence model.

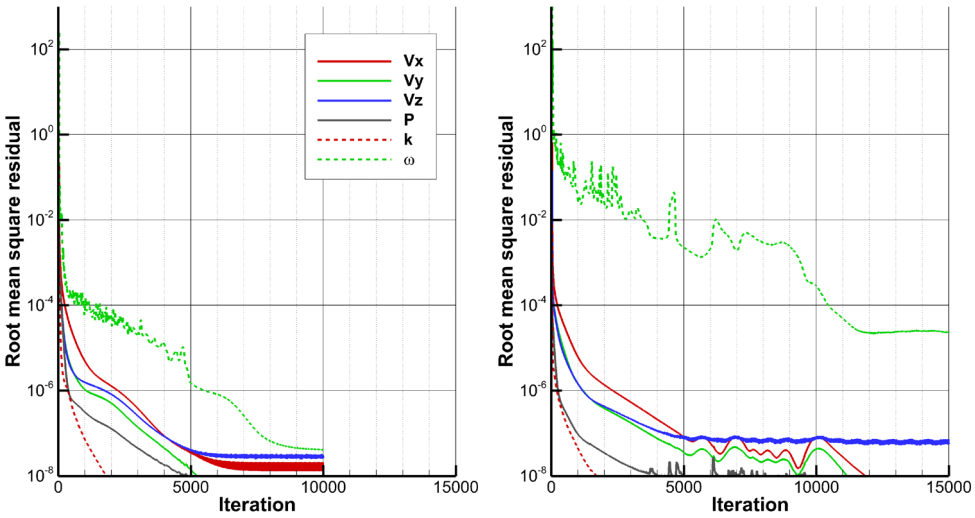


(a) Set 1 - Grid 5 (b) Set 2 - Grid 5

**Figure 5**: Convergence history for with $k-\omega$ $SST$

### 4.2 Forces uncertainty

A direct result of the simulations is the resistance of the ship. The total forces obtained and its components, pressure and friction, are normalized using equation 4:

$$C_i = \frac{F_i}{\frac{1}{2}\rho U_\infty^2 S} \tag{4}$$

Where $i$ is the component of the force, either pressure part, friction part or total, $\rho$ is the fluid density, $U_\infty^2$ is the free-stream velocity and $S$ is the wetted surface of the ship.

The results for the three turbulence models are gathered in table 5 for the first grid set and in table 6 for the second one. In table 7, the experimental results as well as the results obtained by Pereira et al. [2] for structured grids with his finest grid are listed.

For the simulations perfomed with $k-\omega$ $SST$, the pressure drag decreases when the grid is refined while the friction drag increases. Both the friction and pressure drag increase when the wall resolution increases. The same behavior is obtained with $k-\omega$ $TNT$.

For the $k-\sqrt{k}L$, the pressure coefficient shows this similar behavior but the friction drag is highest for the intermediate grids 2 and 3 and decreases slightly for the finest grid.

When comparing the total drag, on average, all simulations underestimate the experimental value. The maximum difference obtained with experimental drag is around 3% for $k-\omega$ $TNT$, 1.5% for $k-\omega$ $TNT$ and 4% for $k-\sqrt{k}L$.

The uncertainty analysis proposed by L. Eça and M. Hoekstra [3] has been performed in order to quantify the discretisation error obtained with these grids. The extrapolation is performed using only the four finest grids of each set, meaning that the grid 1 of each set is not used. For this reason, the uncertainty for grid 1 is not given. The obtained value is only used to show the resulting trend when using coarser grids.

The obtained uncertainties are gathered in table 8 for the first grid set and in table 9 for the second one. For comparison, the uncertainty obtained by Pereira et al. with his finest grid are given at the bottom of each tables.

**Table 5**: $C_p$, $C_f$ and $C_t$ obtained for the first grid set

| Grid | $k-\omega\ SST$ | | | $k-\omega\ TNT$ | | | $k-\sqrt{k}L$ | | |
|---|---|---|---|---|---|---|---|---|---|
| | $C_p$ | $C_f$ | $C_t$ | $C_p$ | $C_f$ | $C_t$ | $C_p$ | $C_f$ | $C_t$ |
| Grid 1 | 0.78 | 3.22 | 4.00 | 0.77 | 3.33 | 4.09 | 0.80 | 3.25 | 4.05 |
| Grid 2 | 0.64 | 3.34 | 3.98 | 0.63 | 3.43 | 4.05 | 0.65 | 3.29 | 3.94 |
| Grid 3 | 0.62 | 3.37 | 3.99 | 0.61 | 3.47 | 4.07 | 0.62 | 3.29 | 3.91 |
| Grid 4 | 0.62 | 3.38 | 4.00 | 0.61 | 3.49 | 4.09 | 0.61 | 3.27 | 3.89 |
| Grid 5 | 0.63 | 3.38 | 4.01 | 0.62 | 3.49 | 4.11 | 0.61 | 3.27 | 3.88 |

**Table 6**: $C_p$, $C_f$ and $C_t$ obtained for the second grid set

| Grid | $k-\omega\ SST$ | | | $k-\omega\ TNT$ | | | $k-\sqrt{k}L$ | | |
|---|---|---|---|---|---|---|---|---|---|
| | $C_p$ | $C_f$ | $C_t$ | $C_p$ | $C_f$ | $C_t$ | $C_p$ | $C_f$ | $C_t$ |
| Grid 1 | 0.80 | 3.38 | 4.19 | 0.80 | 3.48 | 4.28 | 0.79 | 3.28 | 4.07 |
| Grid 2 | 0.65 | 3.43 | 4.08 | 0.64 | 3.52 | 4.16 | 0.65 | 3.31 | 3.95 |
| Grid 3 | 0.63 | 3.43 | 4.05 | 0.62 | 3.52 | 4.14 | 0.62 | 3.29 | 3.91 |
| Grid 4 | 0.62 | 3.43 | 4.05 | 0.61 | 3.54 | 4.15 | 0.61 | 3.28 | 3.89 |
| Grid 5 | 0.64 | 3.42 | 4.05 | 0.63 | 3.53 | 4.16 | 0.61 | 3.27 | 3.87 |

**Table 7**: $C_p$, $C_f$ and $C_t$ obtained by Pereira et al. and $C_t$ obtained experimentaly (EFD)

| Case | $C_p$ | $C_f$ | $C_t$ |
|---|---|---|---|
| Pereira et al. $k-\omega\ SST$ | 0.68 | 3.38 | 4.06 |
| Pereira et al. $k-\omega\ TNT$ | 0.66 | 3.47 | 4.13 |
| Pereira et al. $k-\sqrt{k}L$ | 0.66 | 3.33 | 3.98 |
| EFD | - | - | 4.11 |

**Table 8**: Uncertainties, in percent, obtained for $C_p$, $C_f$ and $C_t$ with the first grid set

| Grid | $k-\omega\ SST$ | | | $k-\omega\ TNT$ | | | $k-\sqrt{k}L$ | | |
|---|---|---|---|---|---|---|---|---|---|
| | $C_p$ | $C_f$ | $C_t$ | $C_p$ | $C_f$ | $C_t$ | $C_p$ | $C_f$ | $C_t$ |
| Grid 2 | 26.7 | 5.0 | 4.1 | 40.9 | 3.4 | 13.3 | 24.0 | 11.2 | 6.2 |
| Grid 3 | 38.8 | 2.5 | 2.9 | 53.7 | 2.0 | 12.1 | 12.5 | 11.1 | 5.2 |
| Grid 4 | 38.0 | 1.4 | 2.4 | 51.1 | 1.4 | 10.4 | 8.0 | 9.9 | 4.6 |
| Grid 5 | 34.0 | 1.0 | 2.0 | 45.1 | 1.0 | 9.0 | 5.8 | 8.7 | 4.1 |
| Pereira et al. | 0.95 | 1.7 | 1.5 | 4.0 | 1.1 | 1.6 | 2.2 | 0.9 | 1.0 |

**Table 9**: Uncertainties, in percent, obtained for $C_p$, $C_f$ and $C_t$ with the second grid set

| Grid | $k-\omega\ SST$ | | | $k-\omega\ TNT$ | | | $k-\sqrt{k}L$ | | |
|---|---|---|---|---|---|---|---|---|---|
| | $C_p$ | $C_f$ | $C_t$ | $C_p$ | $C_f$ | $C_t$ | $C_p$ | $C_f$ | $C_t$ |
| Grid 2 | 20.7 | 1.8 | 2.5 | 29.0 | 2.3 | 7.3 | 11.2 | 5.9 | 4.2 |
| Grid 3 | 33.8 | 1.4 | 1.3 | 41.6 | 1.7 | 8.7 | 6.6 | 4.1 | 2.9 |
| Grid 4 | 33.8 | 1.6 | 0.8 | 40.5 | 1.3 | 8.1 | 4.9 | 3.3 | 2.2 |
| Grid 5 | 30.4 | 1.5 | 0.6 | 35.9 | 1.0 | 7.2 | 3.5 | 2.7 | 1.7 |
| Pereira et al. | 0.95 | 1.7 | 1.5 | 4.0 | 1.1 | 1.6 | 2.2 | 0.9 | 1.0 |

The results show that, for the $k-\omega$ based models, a very large uncertainty is predicted for the pressure part of the force while the values obtained for the $k-\sqrt{k}L$ are much lower. It should be also noted that the pressure contribution is relatively small compared to the friction contribution, which shows values between 1 and 3 % for the $k-\omega$ based models and between 3 and 5 % for the $k-\sqrt{k}L$. The uncertainty predicted on the total drag shows that overall, $k-\omega\ SST$ leads to less uncertainty than $k-\omega\ TNT$ and $k-\sqrt{k}L$ is placed between these two models.

Compared to the results obtained by Pereira et al., the uncertainties obtained for the $k-\omega$ based models for the pressure are much larger while they are in the same range for the friction. For $k-\omega\ SST$, the uncertainty on the total force is also in the same range but they are 4 to 5 times higher for $k-\omega\ TNT$. For the $k-\sqrt{k}L$ model, the results are higher for all the components.

Putting these uncertainties in the perpective of the total drag calculated, we see that $k-\omega\ SST$ leads to the lowest numerical uncertainty, around 2.5 % , but the drag calculated is underestimated. Using $k-\omega\ TNT$ leads to a total drag prediction closer to the experimental data but the numerical uncertainty, around 9 % on average, is much higher than with the $k-\omega\ SST$. The uncertainty obtained with $k-\sqrt{k}L$ is between between the two $k-\omega$ based models with around 4 %, but the drag calculated is the most underestimated.

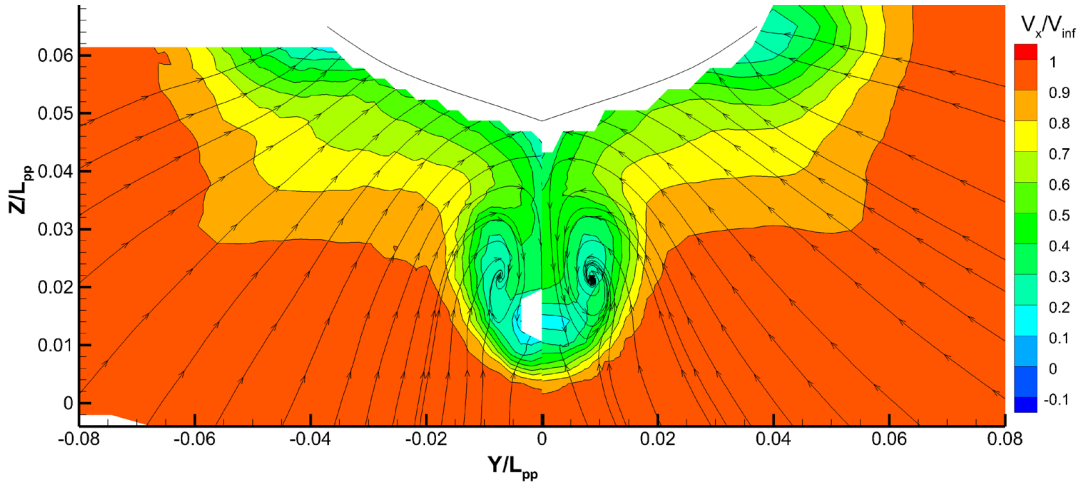


**Figure 6**: Experimental results obtained in the towing tank (left) and wind tunnel (right)

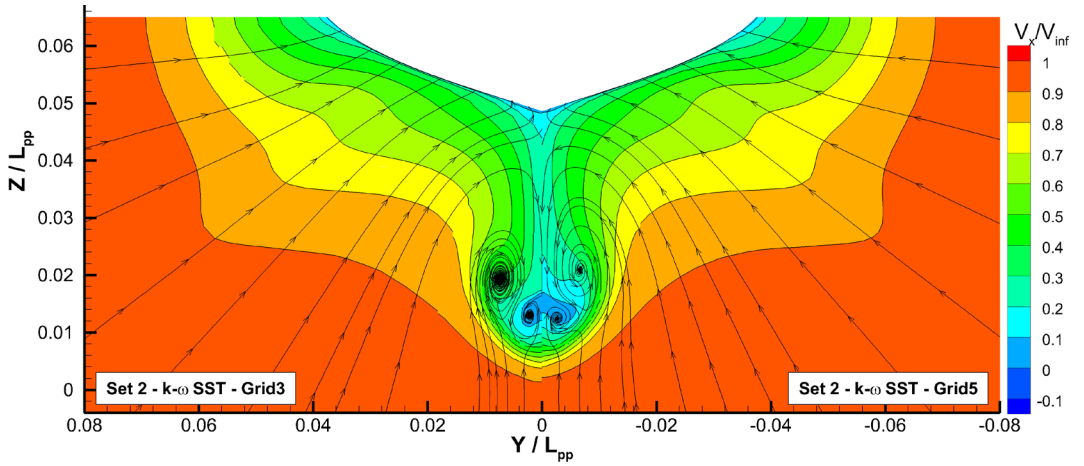


**Figure 7**: Wake flow obtained with $k-\omega\ SST$ with grids 3 (left) and 5 (right) from the second set

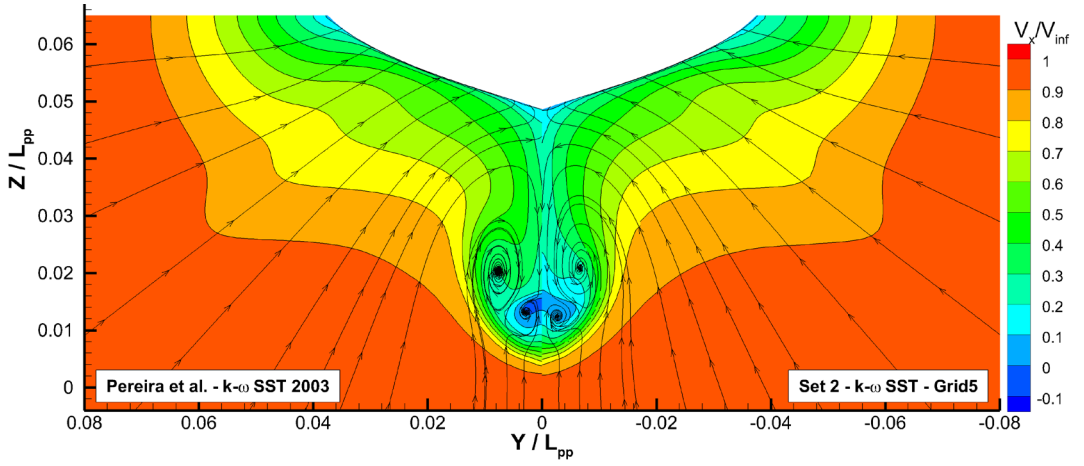


**Figure 8**: Results obtained by Pereira et al. with $k-\omega\ SST$ compared to $5^{\text{th}}$ grid of second set with $k-\omega\ SST$

### 4.3 Wake flow

While the focus so far has been the verification of the integral values obtained with the simulations, the wake flow is also a point of interest. When coupling a propeller analysis to the resistance simulations in order to predict the power requirements of the ship, the proper prediction of the wake flow is crucial.

Figure 6 shows the axial velocity contours and transverse velocity vectors obtained during the experiment carried out by Kim et al.[8] and Lee et al.[9] in a towing tank and windtunnel respectively. The noticeable features of this wake flow are its hook shape and the vortex in the hook.

Figure 7 shows the obtained results with $k-\omega\ SST$ with grids three and five of the second set . It shows that the bilge vortex is present in the wake but the hook shape is entirely smoothed, in grid three, if not missing, in grid five. Figure 8 shows a comparison of the results obtained by Pereira et al. with the results of this study. In the results of Pereira at al. the hook shape is more visible but still not as pronounced as in the experimental results. Figure 8 also shows that the boundary layer near the symmetry plane is thicker in the present study. The velocities further away of the hook shape are similar.

## 5 CONCLUSIONS

In this study, a method to obtain trimmed grids as geometrically similar as possible was presented and applied to the flow around the KVLCC2 at model scale Reynold number. Two sets of five grids with different contractions towards the ship were built, and computations using three different turbulence models were carried out. The obtained integral results were analysed using the method proposed by L. Eça and M. Hoekstra to estimate the discretisation error made. The analysis shows that the numerical uncertainty decreases when using grids with a higher contraction towards the ship.

A grid with reasonable density like Grid3, when using the $k-\omega\ SST$ turbulence model, results in 3% uncertainty on the total drag for the first set and 1.3% for the second set. With $k-\omega\ TNT$ these values increase respectively to 12% and 8.7%. The uncertainty obtained with the $k-\sqrt{k}L$ model are between the two $k-\omega$ based model with 5.2% with the first set and 3% with the second set.

When taking into account only the difference with the force obtained during the experiments, the $k-\omega\ TNT$ model performs overall better than $k-\omega\ SST$ which performs better than the $k-\sqrt{k}L$ model. The $k-\omega\ TNT$ is on average within 1% of difference with the experimental value, $k-\omega\ SST$ within 2% to 3% and $k-\sqrt{k}L$ within 4% to 5%. Compared to the results obtained by Pereira et al. for the same exercise on structured grids, the uncertainty obtained in the present study are larger but the difference with the experiment are in the same order of magnitude and show the same trend.

The analysis of the velocity field in the wake of the ship shows that the grids used in this study are able to capture the bilge vortex, but the hook shape visible in the axial velocity field is smoothed out. More details of this hook shape were captured in the results of Pereira et al. with structured grids in combination with the turbulence models used in that study, but the deviation from the experiements are still pronounced.

The results of this study show that the numerical uncertainty and calculated drag are highly

dependent on the turbulence model used. Using unstructured grids results in more uncertainty than using structured grids even though, for the integrated values, the difference with the exprimments are still contained in the same order of magnitude. Considering the wake flow prediction, the grids used in this study do not permit to capture the flow details at the same level as the structured grids, but turbulence modelling also plays a major role and needs to be adressed in more detail.

## 6 ACKNOWLEGEMENTS

This research is partly funded by the Dutch Ministry of Economic Affairs.

## REFERENCES

[1] www.refresco.org

[2] F.S. Pereira, L. Eça. and G. Vaz. Verification and Validation Exercises for the Flow Around the KVLCC2 Tanker at Model and Full-Scale Reynolds Numbers. *Ocean Engineering*,(accepted for publication)

[3] L. Eça. and M. Hoekstra. A procedure for the estimation of the numerical uncertainty of cfd calculations based on grid refinement studies. *Journal of Computational Physics*, (2014) **262**:104-130

[4] P. Roache. Verification of codes and calculations. *AIAA Journal*, **5**:696-702, Vol. 36, (1998).

[5] F. R. Menter. Ten Years of Industrial Experience with the SST Turbulence Model. *Turbulence, Heat and Mass Transfer 4*, **625-632**, (2003).

[6] J.C. Kok. Resolving the Dependence on Freestream Values for the $k-\omega$ Turbulence Model. *American Institute of Aeronautics and Astronautics (AIAA) Journal*, **38(7)**:1292-1295, (2000).

[7] F. R. Menter, Y. Egorov, and D. Rusch. Steady and Unsteady Flow Modelling Using $k-\sqrt{k}L$ Model". *5th International Symposium on Turbulence, Heat and Mass Transfer*, (2006).

[8] W. J. Kim, S. H. Van, and D. H. Kim. Measurement of Flows Around Modern Commercial Ship Models. *Experiments in Fluids*, 31(5):567:578, (2001).

[9] S. J. Lee, H. R. Kim, W. J. Kim and S. H. Van. Wind Tunnel Test on Flow Characteristics of the KRISO 3,600 TEU Containership and 300K VLCC Double-Deck Ship Models". *Journal of Ship Research*, **47(1)**:24-38, (2003)